Available online at www.sciencedirect.com
ScienceDirect
International Journal of Heat and Fluid Flow 28 (2007) 374–387
International Journal of HEAT AND FLUID FLOW
www.elsevier.com/locate/ijhff

Potential of flow pre-whirl at the compressor inlet of automotive engine turbochargers to enlarge surge margin and overcome packaging limitations ☆

J. Galindo [a], J.R. Serrano [a,*], X. Margot [a], A. Tiseira [a,1], N. Schorn [b], H. Kindl [b]

[a] CMT-Motores Térmicos, Universidad Politécnica de Valencia, Camino de Vera, s/n. 46022 Valencia, Spain
[b] Ford Forschungszentrum, Suesterfeldstrasse 200, 52072 Aachen, Germany

Received 23 June 2005; received in revised form 3 June 2006; accepted 14 June 2006
Available online 4 August 2006

Abstract

Due to the packaging constraints to which turbocharged engines are submitted in passenger cars, the inlet duct of the centrifugal compressor often requires a 90° bend. The compressor inlet perpendicular to its axis disturbs the flow and reduces the compressor performance. This paper presents an interesting solution based on a specifically designed inlet swirl-generator device (SGD) that palliates these negative effects. In addition, the SGD can be used to extend the surge margin of the compressor if the position of the SGD blades is modified in function of the reciprocating engine operation conditions. The paper describes how the swirl level and the pressure losses generated by the device have been characterized in a continuous flow test rig. After this the SGD plus a centrifugal compressor from a turbocharger unit have been tested in a specific turbocharger test bench. The results obtained show the influence of the SGD blades position on the compressor performance. In order to better understand the influence of the SGD on the turbocharger behaviour, the flow velocity triangles near the inducer have been reconstructed using an approach based on CFD calculations.

Keywords: Turbocharging; Turbocharger; Compressor surge; Centrifugal compressor; Car packaging

1. Introduction

Turbocharging Diesel engines is one of the most effective techniques for increasing their performance while reducing pollutants and CO_2 emissions (or fuel consumption). The advantages of turbocharging are not only limited to maintaining acceptable air to fuel ratios with high fuel injected levels. Furthermore, it allows increasing the air density inside the cylinders, which is an efficient technique to accelerate the atomization and mixture of the injected fuel as stated by Binder and Schwarz (2004). In addition, since the density of the trapped air is increased, the fuel jets penetrate less inside the cylinders, and this is especially important for improving the HC and soot emissions in HSDI Diesel engines, particularly in consideration of the actual downsizing trends and the consequent risks of fuel jet impingement on the walls of the cylinder (Araneo et al., 1999). The improvements on fuel mixture and atomisation due to the higher in-cylinder density allow the reduction of air to fuel ratios tolerated by Diesel engines, which bring about an improvement of the engine performance much more important than the increase obtained with the engine air load density.

However, turbocharging has some limitations such as the turbocharger lag, mainly caused by the necessity to overcome the mechanical inertia of the turbochargers, and which is responsible for the delay in air density

☆ This work has been partially supported by the Generalitat Valenciana. Grants CTIDIA/2002/17 and GV06/057.
* Corresponding author. Tel.: +34 96 387 96 57; fax: +34 96 387 76 59.
E-mail address: jrserran@mot.upv.es (J.R. Serrano).
[1] This co-author is supported by a FPI grant from the Generalitat Valenciana.

0142-727X/$ - see front matter © 2006 Elsevier Inc. All rights reserved.
doi:10.1016/j.ijheatfluidflow.2006.06.002

Nomenclature

A_d	geometrical transversal section of a duct
C	absolute inlet velocity
c_D	discharge coefficient
D	diameter
g	angle of attack
i	incidence angle
I_{cyl}	moment of inertia
K	pressure loss coefficient
M	torque
$\dot{m}$	mass flow rate
p	pressure
R	perfect gas constant
T	temperature
U	rotor tangential velocity
W	absolute relative velocity
W_c	compressor work
α	angle of inlet absolute velocity
β	angle of SGD vane aperture
ϕ	approach angle
γ	ratio of heat capacities, 1.4
λ	angle of swirl
π_c	compression ratio
ρ	density
ω_{air}	angular air velocity

Subscripts

0	stagnation conditions
1	compressor inlet
2	compressor outlet
a	axial
e	exit
ed	exit duct
i	inlet
id	inlet duct
r	real
s	isentropic
sw	swirl meter
t	theoretical
u	tangential

Acronyms

CFD	computational fluid dynamics
HSDI	high speed direct injection
IGV	inlet guide vanes
SGD	swirl generator device
VGT	variable geometry turbine

increase against sudden load demands of the engine (Watson and Janota, 1982). Another drawback is due to the intrinsic limits of a given compressor map: surge and choke. The surge can limit the pressure ratio capability when the engine is working at low speed and high load (low end torque). It is then necessary to improve the behaviour of the compressors for small flow rates in order to extend the torque range. At rated power the compressor choke limitations can cause over-speed of the turbocharger, especially when the engine is operating in altitude with reduced atmospheric pressure. Hence, a correct matching between the turbocharger and the Diesel engine is essential to achieve maximum performance with turbocharging (Tange et al., 2003; Chen and Connor, 2002; Theotokatos and Kyrtatos, 1997).

The bibliography lists different ways of extending the range of operation and of improving compressor performance. In some studies aimed at moving the surge line the geometry of the diffuser is varied and its interaction with the volute analysed (Gu et al., 2001; Ludtke, 1983). In small centrifugal compressors different devices are used for axial pipe inlets, like for instance a bleed system that provides a secondary inlet around the primary one (Hunzinker et al., 2001). Other systems described by Meherwan Boyce (2002), Coppinger and Swain (2000) and Whitfield et al. (1975) include the inlet guides vanes (IGV) which develop a positive pre-rotation in the flow that enters in the inducer or even the jets to simulate inlet pre-whirl, as proposed by Kyrtatos and Watson (1980), along with inlet blockage.

Another drawback for the integration of the turbocharger in passenger cars is due to the strict packaging requirements for the engine and its accessories, which often force to place the compressor inlet at 90° with respect to its axis. As a consequence, the flow cannot enter in the compressor inducer in optimal conditions (Kim et al., 2001; Ariga et al., 1983). This is illustrated in Fig. 1 where the space available for the inlet piping to the compressor, in the real case used for this work, is indicated.

A 90° inlet configuration placed near the inducer impellers generates a non-uniform entry flow (Schulte et al., 2004). Talib et al. (1992) studied the effect of flow rate instabilities on loss mechanisms in a backswept centrifugal impeller and obtained similar conclusions. Fink et al. (1992), Hansen et al. (1981), Ariga et al. (1987) and Elder and Gill (1985) separate the non-uniform flow into two cases, radial and circumferential and they state that these discontinuities can be the cause of undesirable instabilities in the operation of the compressor. From previous studies it seems clear that in order to maintain the performance in the centrifugal compressor and dispose of an ample margin for the compressor operation, especially near the surge line, it is necessary to have a uniform flow at the compressor inducer. For this reason a solution is proposed in this paper to smoothen the distortions by fitting a swirl generation device (SGD) in the reduced space allocated in the vehicle.

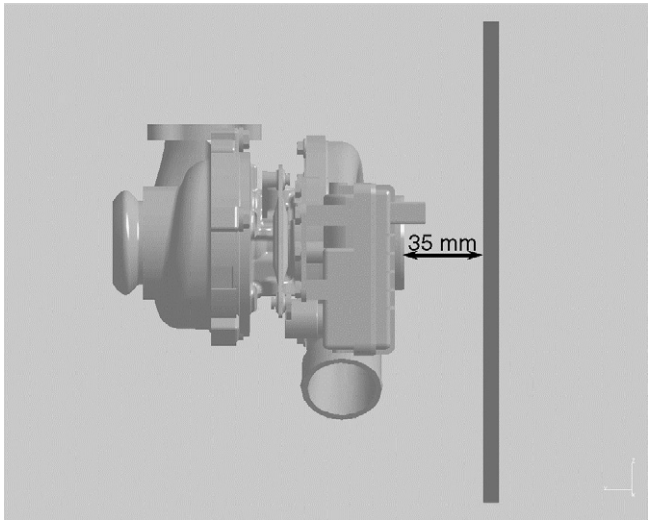

Fig. 1. Turbocharger with the boundary representing the packaging requirements.

The SGD replaces the 90° bend that would normally link the engine intake line to the compressor and has to fit in the space left between the housing and the compressor entry (Fig. 1). It is expected that the SGD improves the flow uniformity and in addition it could be used to extend the compressor stable operative range.

Though the SGD seems similar to an IGV device, the way in which the SGD modifies the flow field at the compressor inlet is very different. Therefore, the way in which both devices affect the compressor performance is essentially not the same. Indeed, the main objective of this paper is to explain the measured variations in the operative map and efficiency of a centrifugal compressor when there is a SGD mechanism upstream.

The following methodology has been used for this work: Firstly, the SGD has been designed with the help of a CFD code and manufactured accordingly. Secondly, the SGD has been characterised in a continuous flow test rig in order to measure its ability to generate swirl as a function of several operative parameters like the air mass flow or the position of the SGD blades. Then, the SGD has been installed at the compressor inlet of a turbocharger, in the turbochargers test bench described by Luján et al. (2002) and the compressor performance maps have been measured with different SGD vane apertures, i.e. at different swirl angle values. A measurement of the compressor map has also been performed with an axial inlet configuration (i.e. with no additional element upstream of the compressor) to serve as a reference for the analysis of the SGD influence. The modifications in the surge line obtained with the SGD have been explained through the analysis of the velocity triangles at the compressor inlet. These have been reconstructed using the information about the airflow field at the SGD outlet obtained from CFD calculations. The CFD calculations have been compared with the measurements from the SGD characterization in the continuous flow test rig in order to assess the realism of the CFD predictions. Finally the conclusions about the behaviour of the SGD and the optimal operation conditions, to match the turbocharger with the Diesel engine, are exposed.

2. Design and manufacturing of the SGD

In order to design the SGD different CFD studies, which have been described in detail by Schulte et al. (2004), have been performed. It was designed to fit between the intake line and the compressor inlet, oriented at 90° from the intake due to packaging constraints. In general, the following geometric conditions have to be imposed to define the outer geometry:

- The overall diameter of the SGD should not exceed the compressor housing diameter.
- The SGD outlet diameter is defined by the compressor inlet diameter (39.2 mm in the studied case).
- The maximum SGD thickness will be generally limited by the packaging constraints (35 mm in the studied case, Fig. 1) and the rectangular inlet flow area of the SGD has to be equal to the compressor inlet section. Therefore, the length and height of the rectangle that forms the inlet flow area have to be chosen according to previous limitations.

The final adopted geometry is shown in Fig. 2a, and has the following main characteristics: The rectangular inlet flow area ($16 \times 75\ mm^2$) was defined to be same as the SGD outlet area, with its width imposed by the limited space available. An outer radius of curvature of 1.5 mm was imposed to smoothen the brusque change in direction. The distance between the SGD outlet and the compressor inducer inlet is 45 mm. The volute type inlet was chosen as the best option to minimise pressure losses (Pan et al., 1999; Qi et al., 1996). A configuration with 10 blades, each of length 16 mm, was designed based on previous studies of Schulte et al. (2004) aimed at finding the solution with the lowest pressure drop and the maximum swirl level.

The SGD has been manufactured in a hard plastic material and is formed by a case containing the blades and a lid. The 10 blades of the SGD are placed in holes especially prepared in the lid and the case and fastened to the case with soldered screw shafts. Fig. 2b shows an open view of the SGD as well as a side view of the assembly between the compressor inlet and the SGD. The SGD blades angle (β in Fig. 2a) had to be changed and fixed individually and manually. It was possible to impose the direction of rotation by forcing the outlet flow through either the case (positive rotor compressor direction) or the lid (negative), covering one of the exits. Hence the SGD can provide positive or negative swirl.

3. Characterisation of the SGD in a continuous flow test rig

To characterise the SGD a continuous flow test rig is used. This experimental facility has been designed and

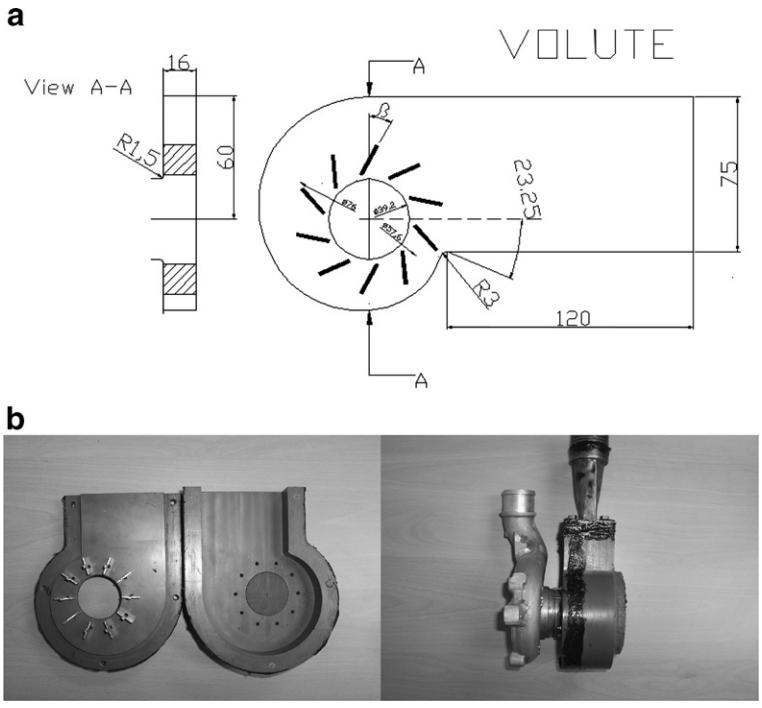

Fig. 2. (a) Geometry of the swirl generator with aperture angle β (dimensions in mm). (b) Two different views of the SGD.

used, following the guidance of Arcoumanis and Whitelaw (1987), to determine the swirl and the permeability of cylinder heads of internal combustion engines working with steady and unsteady flows (Desantes et al., 1995). The flow test rig is therefore considered the ideal facility to determine, not only the angle of swirl (λ) for different values of the SGD vanes aperture, but also to calculate the pressure loss through the SGD.

The methodology to obtain the pressure loss caused by the SGD was developed in the works of Arcoumanis and Whitelaw (1987) and Desantes et al. (1995) in order to determine engine cylinder head permeability and was adapted here to the SGD. It is based on two experiments. The first one consists in measuring the pressure drop and mass flow rate through a line formed only by the SGD inlet and outlet ducts and the swirl meter but without the SGD. Its purpose is to determine the pressure loss coefficient of the flow between the inlet and the complete line normally connected to the SGD. The result is the global pressure loss coefficient K_A in Eq. (1). In the second experiment the SGD is mounted and the pressure loss coefficient of the whole set-up is determined, the result is K_B in Eq. (2). The configuration with the SGD is shown in Fig. 3a. The difference between both coefficients yields the loss coefficient of the SGD, K_{SGD} in Eq. (3), and finally the pressure loss of the SGD (Δp_{SGD}) is calculated from Eq. (4).

$$K_A = K_i + K_{id} + K_{sw} + K_{ed} + K_e \quad (1)$$

$$K_B = K_i + K_{id} + K_{sw} + K_{SGD} + K_{ed} + K_e \quad (2)$$

$$K_{SGD} = K_B - K_A \quad (3)$$

$$\Delta p_{SGD} = \frac{1}{2} K_{SGD} \frac{1}{\rho_{atm}} \left(\frac{\dot{m}_r}{A_d}\right)^2 \quad (4)$$

This procedure is repeated for different vane apertures to obtain the pressure loss of the SGD in function of the angle β. These equations are limited to the incompressible flow, i.e. for Mach numbers of less than 0.3. In the continuous flow test rig the mass flow rate has been varied from 0 kg/s to the maximum value possible at each vane aperture. In Fig. 3b the variation of Δp_{SGD} shows that the pressure drop is more significant and steeper for large values of the angle β and it increases with the mass flow rate. As may be also observed, the higher permeability does not correspond to 0° of SGD vane angle but to 15°, and this is due to the non-symmetric design of the SGD. In fact, the optimum permeability is actually expected for a β value between 0° and 30°.

Following the analysis of the experimental results obtained in the flow test rig, it is possible to calculate a discharge coefficient (c_D) of the SGD defined in Eq. (5), as the ratio between the measured mass flow rate through the SGD and the theoretical mass flow rate that could pass through the geometrical section of the SGD outlet in an isentropic expansion, defined with Eq. (6).

$$c_D = \frac{\dot{m}_r}{\dot{m}_t} \quad (5)$$

$$\dot{m} \cdot \frac{\sqrt{\gamma R T_{i0}}}{p_{i0}} = A_{eff} \cdot \gamma \cdot \left(\frac{p_e}{p_{i0}}\right)^{1/\gamma} \cdot \sqrt{\frac{2}{\gamma - 1} \cdot \left[1 - \left(\frac{p_e}{p_{i0}}\right)^{(\gamma-1)/\gamma}\right]} \quad (6)$$

The values of this coefficient are represented in Fig. 3c for different vane apertures and versus the measured air mass flow rate. It can be observed that as the aperture of the SGD decreases, i.e. for higher β values, the c_D value

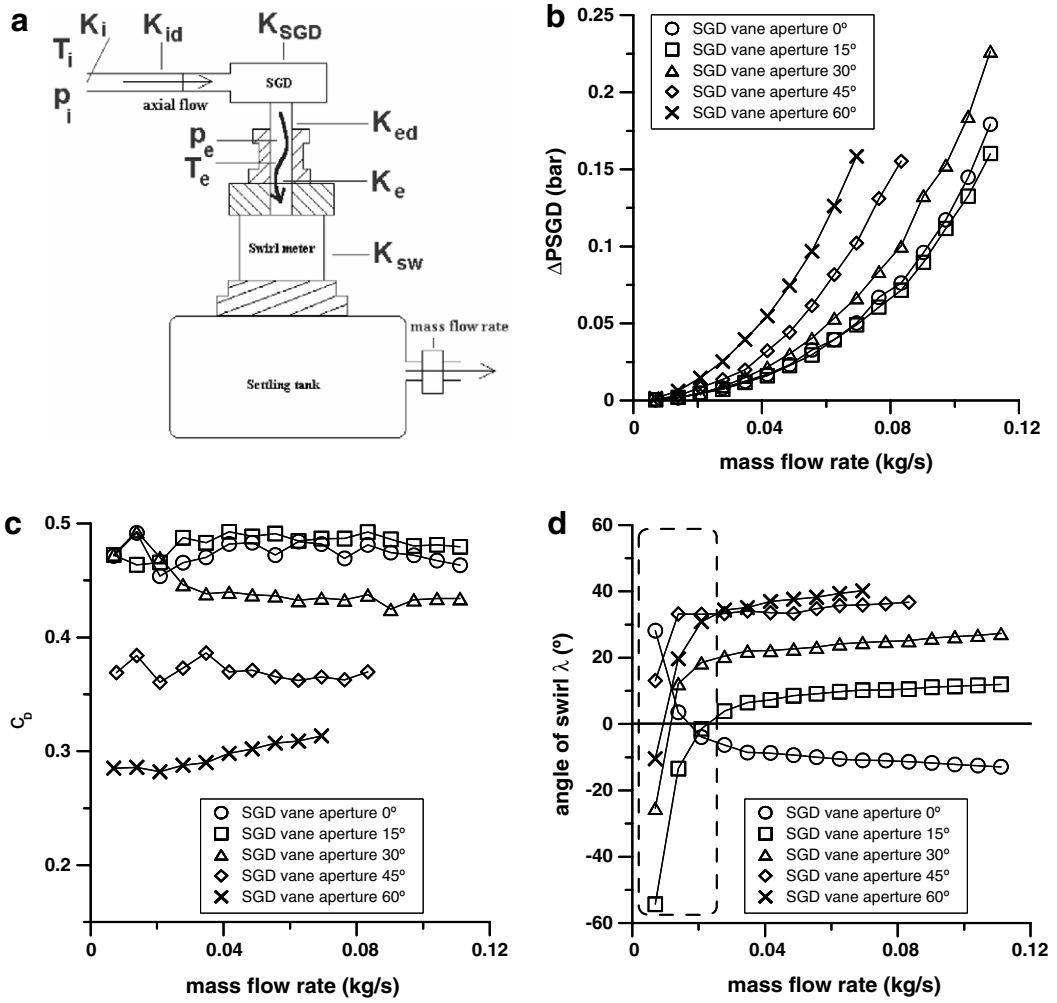

Fig. 3. Flow test rig characterisation of SGD: experimental set-up, results of measurements for various vane apertures and comparison with CFD calculations.

decreases, due to the reduction of the effective area used by the flow. For β values of 0°, 15° and 30° and at the lowest air mass flow rates (below 0.025 kg/s) the pressure drop in the SGD is very low (Fig. 3b) and therefore the uncertainties in the calculation of c_D with Eqs. (5) and (6) are very high, as can also be observed in Fig. 3c.

Finally, the tests in the continuous flow test rig served to determine the level of swirl generated. The angle of swirl is not equal to angle β. An impulse swirl meter was used (Fig. 3a) to determine the angle of flow rotation. It consists of a honeycomb matrix that is suspended by a frame over the settling tank and normal to its axis. The angular momentum of the descending air is totally destroyed by the matrix so that the resulting torque on it is numerically equal to the angular momentum flux. Torques of up to 0.1 N m, of either positive or negative polarity can be measured. Using the hypothesis that assimilates the flow in the duct to a cylindrical rigid solid spinning around its axle, the expression of the torque is obtained, Eq. (7), and the angular velocity of the cylinder can be calculated by Eq. (8):

$$M = I_{\mathrm{cyl}} \cdot \omega_{\mathrm{air}} \frac{\dot{m}_{\mathrm{r}} \cdot D^2}{8} \cdot \omega_{\mathrm{air}} \tag{7}$$

$$\omega_{\mathrm{air}} = \frac{8 \cdot M}{\dot{m}_{\mathrm{r}} \cdot D^2} \tag{8}$$

The tangential velocity in the periphery of the cylinder is then calculated by the equation:

$$C_{1\mathrm{u}} = \omega_{\mathrm{air}} \frac{D}{2} = \frac{4 \cdot M}{\dot{m}_{\mathrm{r}} \cdot D} \tag{9}$$

The axial velocity C_{a} is calculated from the equation of continuity but considering that the effective section at the SGD outlet is reduced by taking into account the c_D coefficient, Eq. (10).

$$C_{1\mathrm{a}} = \frac{4 \cdot \dot{m}_{\mathrm{r}}}{\pi \cdot \rho \cdot D^2 \cdot c_{\mathrm{D}}} \tag{10}$$

The angle of rotation of the flow (λ) is then defined as the ratio of $C_{1\mathrm{u}}$ and $C_{1\mathrm{a}}$:

$$\lambda = \arctan \frac{C_{1\mathrm{u}}}{C_{1\mathrm{a}}} = \arctan \frac{\pi \cdot \rho \cdot M \cdot D \cdot c_{\mathrm{D}}}{\dot{m}_{\mathrm{r}}^2} \tag{11}$$

The different levels of swirl obtained for various positions of the SGD vanes (Fig. 3d) show that for values of the mass flow rate greater than 0.025 kg/s the angle remains approximately constant with the mass flow rate, although for values lower than 0.025 kg/s, or near this point, the angle of swirl suffers a very large dispersion. The reason is that for such a low air mass flow the friction forces are comparatively high with respect to the angular momentum of the flow and the torque meter measurements cease to be accurate. As a consequence, with very low values of torque and mass flow any error is amplified in the calculation of Eq. (11).

4. Description of the experimental study in the turbocharger test bench

A turbocharger test bench prepared to measure compressor and turbine maps has been used to characterise the SGD coupled to a centrifugal compressor. A detailed description of this installation can be found in the works of Galindo et al. (2006) and Luján et al. (2002). The SGD is placed upstream of the centrifugal compressor as represented in Fig. 2b. The air mass flow and the thermodynamic variables are measured upstream of the SGD and downstream of the compressor. The testing procedures satisfy SAE Supercharger Testing Standards (1995) and Turbocharger Gas Stand Test Code (1995) and have been also described by Galindo et al. (2006) and Luján et al. (2002). The methodology used in all tests remained the same, i.e. the SGD was placed upstream of the inducer with the specified length requirements and the blades of the SGD were manually fitted and tightened with nuts in the desired position (Fig. 2b). Using the characterization of the SGD in the flow test rig, it is possible to calculate the value of λ (Eq. (11)), as a function of the β angle and the air mass flow through it (Fig. 3d). The operative variables measured and the corresponding transducers ranges were

- Compressor air mass flow rate: Hot-film anemometer, ranges: 0–0.2 kg/s.
- Upstream and downstream pressure: Average value of two piezo-resistive transducers, absolute pressure range: 0–5 bar.
- Upstream and downstream temperature: Average value of 2–4 thermo-resistances at different immersions, range: 20–1300 °C.

Measurements were performed with three different SGD vane apertures (15°, 30° and 60°) and the axial inlet line was considered as the base line configuration. The maps of the compressor plus the SGD with two different SGD vane apertures are represented in Fig. 4a–d where Fig. 4a is a zoom from Fig. 4b. The pressure ratio of these figures is defined as the ratio between the pressures measured downstream of the compressor and upstream of the SGD respectively. The variables of the maps were corrected with the data measured upstream of the SGD entry. In these maps three constant speed lines (100, 140 and 180 krpm) have been plotted as well as the line that limits the surge area from stable operation. The surge limit line has been defined following the criteria exposed by Galindo et al. (2006). The iso-velocity curves for a given vane aperture, with positive and negative pre-rotation, have been compared with the reference axial flow configuration. According to the maps shown in Fig. 4, the configurations with negative and positive vanes angle yield very similar compression ratios at the lowest air mass flow rates of each speed. This can be explained by Fig. 3d, which shows that the λ value is undefined below 0.025 kg/s due to the very low momentum of the flow, so that in this area of the map the expected swirl has no significant influence in the compressor performance. However, when increasing the air mass flow the negative configuration allows for higher compression ratios than the positive one. In any case the highest compression ratio is always obtained for the axial flow configuration. This is due to the important pressure loss caused by the SGD (Fig. 3b), which is included in the measured maps.

With respect to the variations in the surge margin, it can be concluded from the results of Fig. 4 that the lower β values did not result in any significant improvement of the surge line. This is expected since the λ value is very low and the swirl level undefined in the case of air mass flow rates under 0.025 kg/s (Fig. 3d). For $-60°$ of vanes angle the swirl generated improves the surge line characteristics for compression ratios equal or higher than 1.8. Fig. 4a and b show that the negative pre-whirl setting has more potential than the positive pre-whirl setting. In this case the minimum air mass flow rate for which the compressor is stable has been reduced by about 25% with the negative pre-whirl. Another more interesting way to look at the improvement obtained is that for about 0.026 kg/s of mass flow rate the maximum stable compression ratio has been increased by about 0.45 bar (from 1.88 to 2.33), which represents about 25% of boost pressure increment in this area of the map for a given reciprocating internal combustion engine.

From Fig. 4e–h the total to total isentropic efficiency for different negative and positive pre-whirls at 140 krpm and 180 krpm, respectively are depicted. The curves show that the pressure losses caused by the area reduction in the SGD have a negative influence on the compressor efficiency. As a result, the highest efficiency normally corresponds to the axial inlet flow configuration, except in the case with $+60°$ of SGD vanes angle and the lower range of mass flow rates, as will be explained in the next section.

5. Analysis and discussion of the experimental results

If the SGD pressure drop measured in the continuous flow test rig (Fig. 3b) is subtracted from the values of the pressure measured upstream of the SGD, in the turbocharger test bench, it is possible to obtain the absolute pressure just upstream of the compressor inducer. Thus the

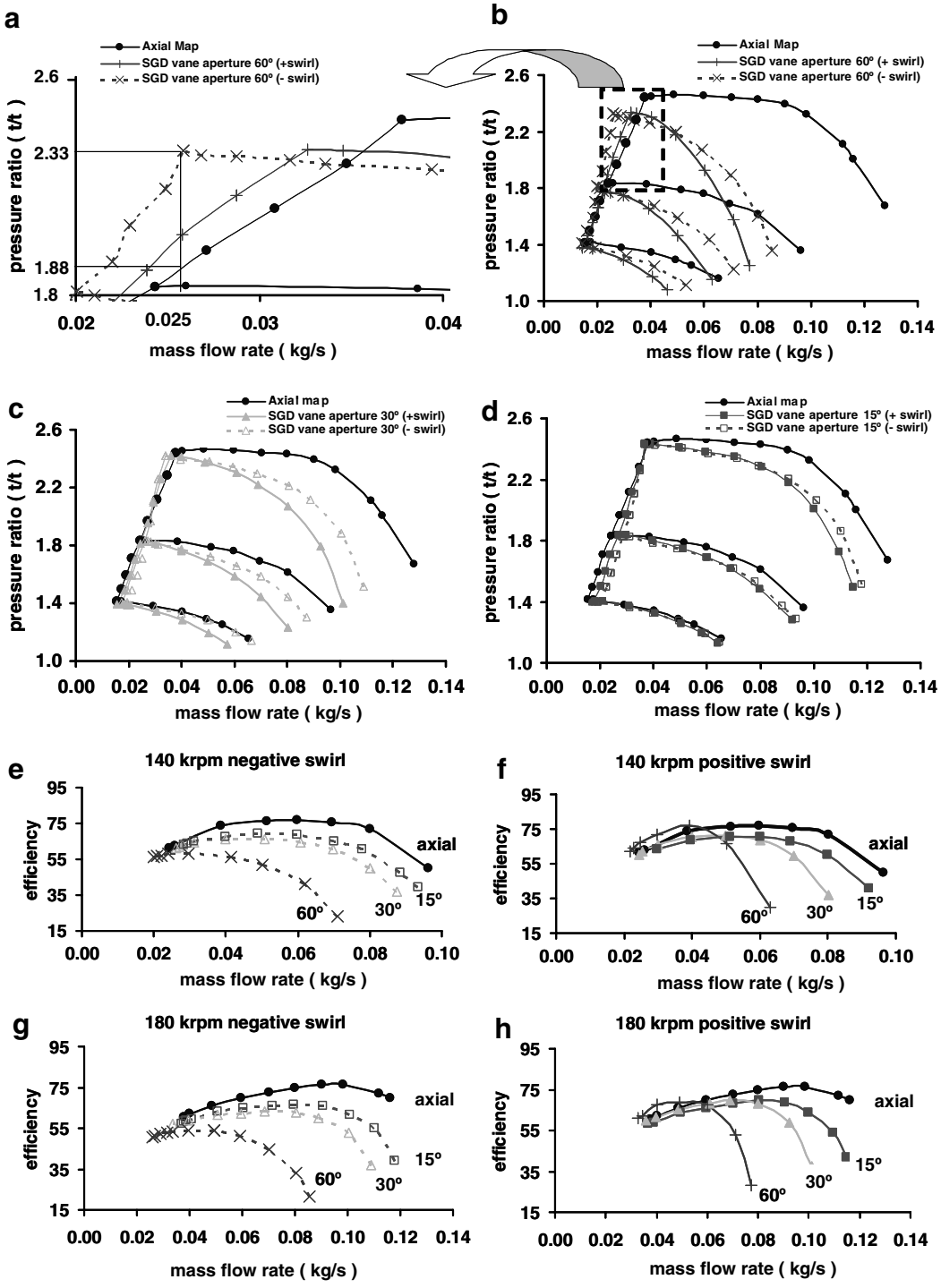

Fig. 4. Compressor maps and isentropic efficiency comparing the axial inlet configuration with ±15°, ±30° and ±60° of SGD vanes position at two different rotating speeds (140 and 180 krpm).

compression ratio can be calculated without the effect of the pressure losses in the SGD. For better understanding in Fig. 5a there is a diagram that shows how the thermodynamic process from point 1 to point 2 changes when the pressure loss value is eliminated. The thermodynamic process from 1′ to 2 is closer to the isentropic evolution, because the calculated point 1′ has lower pressure than the measured point 1, but point 2 does not change.

In addition, in Fig. 5 the compressor maps using the reconstructed pressure upstream of the compressor inducer are shown. When comparing these with Fig. 4, the effect of the SGD pressure losses on the compression ratio and efficiency can be observed.

The maps of Fig. 5 should be coherent with the swirl influence on the velocity vectors at the compressor inducer. Indeed, Fig. 6 shows how the vectors of the velocity trian-

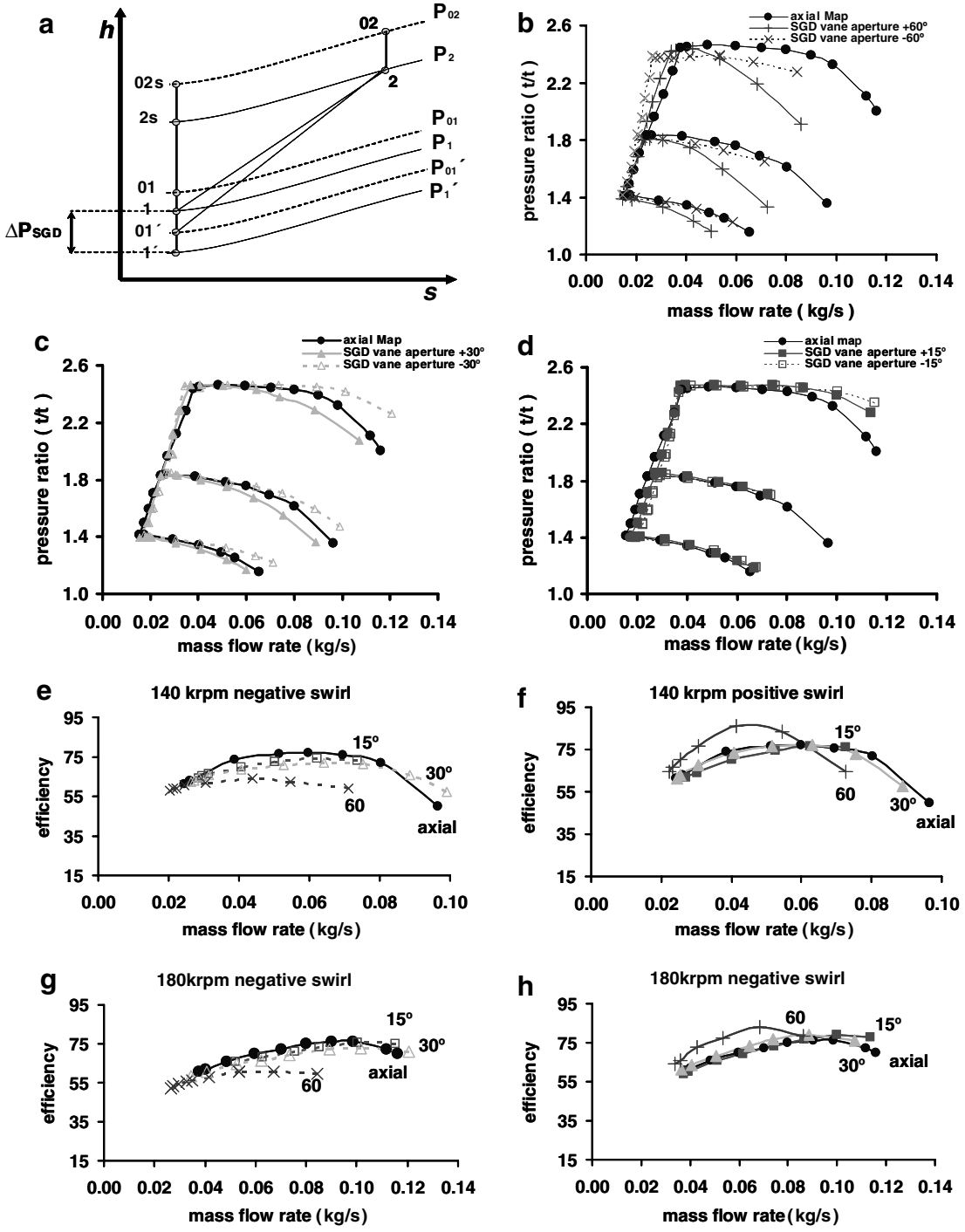

Fig. 5. Compressor maps and isentropic efficiency reconstructed by subtracting the influence of the pressure losses in the SGD.

gles change at the compressor inducer when pre-whirl is imposed, assuming that the air mass flow and the compressor rotating speed are constant in the two cases represented. The increment of the relative velocity (W_1) with negative swirl is significant with respect to the positive case. If the compressor effective work is defined by the Euler equation (12), and constant speed and constant air mass flow conditions are considered, then: U_2, U_1 and C_{2a} are constant. In addition, in conventional analysis the outlet angle of the flow is considered as a geometric characteristic of the exducer blade shape, though this is not rigorously true because the outflow angle should also depend on the flow physics inside the impeller. Hence, the triangle of velocities at the compressor outlet is held constant independently of the inlet swirl flow. As a consequence, the only term that is modified in Eq. (12) is C_{1u}.

$$W_c = U_2 \cdot C_{2u} - U_1 \cdot C_{1u} \tag{12}$$

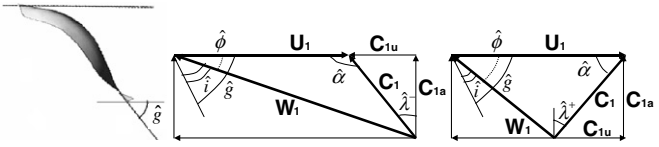

CFD impeller Negativepre-whirl Positive pre-whirl

Fig. 6. Velocity triangles with negative and positive SGD vanes angle at the inlet of the compressor inducer.

Developing this equation yields Eq. (13):

$$W_c = U_2 \cdot C_2 \cdot \cos\alpha_2 - U_1 \cdot C_1 \cdot \cos\alpha_1 \tag{13}$$

Since this equation depends on the sign of $\cos\alpha_1$, it can be deduced that the effective work with positive pre-rotation is smaller than in the axial flow case, which in turn is smaller than with negative pre-rotation, as expressed in relation (14). Thus, for a given temperature at the compressor inlet and a given compression ratio the isentropic efficiency should be higher with positive pre-rotation than with the other two configurations.

$$W_c(\text{positive swirl}) < W_c(\text{axial}) < W_c(\text{negative swirl}) \tag{14}$$

In terms of compression ratio (π_c) follows inequality (15). Indeed, with the positive pre-whirl the relative velocity reduction is smaller (Fig. 6), which implies that the increment of flow pressure is also smaller. In other words, inequality (14) shows that a positive pre-whirl results in a reduction of the work input to the gas, so that the compressor pressure ratio is smaller for a given efficiency and temperature at the compressor inlet.

$$\pi_c(\text{positive swirl}) < \pi_c(\text{axial}) < \pi_c(\text{negative swirl}) \tag{15}$$

The maps calculated with the reconstructed pressure upstream of the compressor inducer and shown in Fig. 5 should confirm relations (14) and (15). However, though it is verified in the cases of −15°, ±30° and +60° of β angle, it is less clear for +15° and −60°. In general, the ±15° cases show very similar pressure ratios and both are quite similar to that of the axial configuration (Fig. 5d), which can be explained by the low swirl level generated. Nevertheless, at 180 krpm and high mass flow rate an increment of the compression ratio can be observed not only with the −15° but also with +15° configuration; due to the increment in the compressor efficiency with respect to the axial case (Fig. 5h). Finally, for the −60° SGD vane aperture the compression ratio obtained is equal or smaller than that of the axial configuration, which is in contradiction to what is predicted by inequality (15). The reason lies again in the lower compressor efficiency with respect to the axial case (Fig. 5e and g). Nevertheless, this configuration yields the best performance for 180 krpm speed with respect to the surge limit line (Fig. 5b), indeed at these low mass flow rates the efficiency measured with −60° and axial configurations are not so different (Fig. 5g).

With respect to the isentropic efficiency, the values shown in Fig. 5f and h for +15° and +30° of β angles are roughly at the same level as those for the axial configuration. However, for the +60° position and the lower air mass flow rates there is a significant increase in isentropic efficiency. This is the reason why the same compression ratio is obtained at the lower air mass flow rates with +60° and axial configuration (Fig. 5b) in spite of the lower work input predicted by inequality (14).

In the case of negative pre-whirl the isentropic efficiency decreases as β angle increases. In the cases with a compression ratio very similar or even lower than the axial configuration, the higher work input predicted by relation (14) explains the lower efficiency obtained.

6. Use of CFD for interpreting the observed measured behaviour

The influence of the different β angle values on the surge line and on overall compressor performance has been verified on the turbocharger test bench. However, the information gathered from CFD calculations brings about a better understanding of the SGD influence in the flow field at the compressor inlet.

The software used for the calculations was Fluent 6.0, with the segregated implicit solver and the standard k–ε turbulence model. Following assumptions were made: First the flow was calculated in steady state conditions to compare with the experimental characterisation performed in the test rig. Secondly the airflow was considered incompressible, based on the low pressure differences between inlet and outlet (about 1500 Pa) imposed by the inflow/outflow pressure boundary conditions; therefore density is constant throughout the domain. Previous verification calculations have shown that this simplification leads to less than 3% error and does not affect the general conclusions of the study performed here.

An unstructured mesh was needed to represent the complex geometry, with finer cells around the blades. Following a mesh independence study the number of cells was set at 80,000. The mesh front view of the SGD, as well as the entry section to the compressor inducer are shown in Fig. 7. The steady state calculations were considered converged when the residuals were of order 10^{-4}, and the mass flow rate as well as the velocity profile at the duct exit were stabilised.

For the CFD calculations the total length of the outlet duct was defined as 176 mm so as to avoid any influence of the boundary conditions on the solution at the compressor entrance section. This is approximately the double of the real length (80 mm) formed by the SGD outlet duct plus the inlet channel to the compressor inducer and marked in Fig. 7.

6.1. Analysis of the CFD results and comparison with the experimental characterization

CFD calculations have been performed for operation conditions close to the surge line of the compressor map,

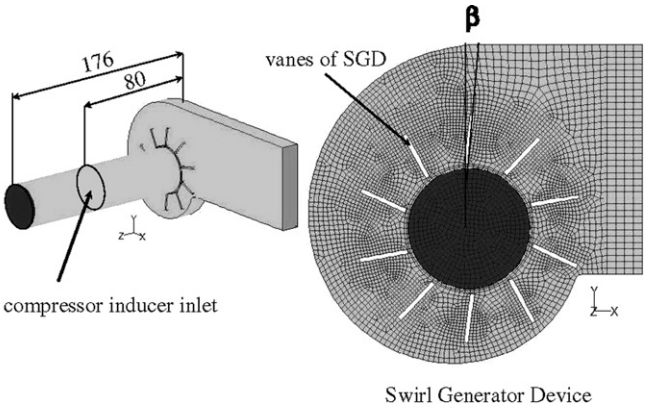

Fig. 7. Geometry and position of the compressor inducer and mesh of the swirl generator with SGD vanes angle (β). Dimensions in mm.

i.e. for a pressure drop of 1500 Pa and a mass flow rate of about 0.03 kg/s, and compared with the experimental results from the continuous flow test rig. The comparison is represented in Fig. 8. The pressure loss coefficient (K_{SGD}) is relatively low and constant up to 30° of β angle, but it increases rapidly as the vanes close, doubling practically from 30° to 60° (Fig. 8a). This is the effect of the area reduction that results from closing the vanes: between 0° and 30°, the vane channel area does not change much, whereas it is considerably reduced for higher β values. When comparing with the experimental results, it is important to remember that in Eqs. (1) and (2) the pressure loss coefficient of the swirl meter K_{sw} is assumed to be the same, though the flow is purely axial in one case and swirling in the other. In fact the losses in the swirl meter depend on the inlet flow conditions and hence on the swirl. Since it is impossible to quantify this effect, it means that the pressure loss calculated with Eq. (4) is lightly overestimated. In addition, the total pressure loss measured in the flow test rig includes that of the coupling element between the cylindrical duct of the standard installation and the rectangular SGD entry. This coupling element, which was not modelled in the CFD calculation, is quite probably the main source of the higher pressure loss observed in the experimental results.

Fig. 8b shows that the swirl increases rapidly, from negative values of around −10° in the radial position of the vanes to values of around 30° at β angle of 45°, and then more asymptotically as the vanes close, to reach about 35° of swirl at 60° β angle. It is worth mentioning that in both the experimental and modelling results the non-swirling flow is obtained for an incidence angle of the vanes of around 10–15°, and that the swirl becomes negative for lower β values. The curve representing the experimental measurements performed on the steady flow test rig confirms the tendency observed in the numerical simulations and in general, good agreement was found between the experimental measurements and the CFD results. The differences observed can be explained by the reduced accuracy of the torque meter at low swirl levels and the possible small deviations of the manual vane angle setting.

The characteristic flow pattern in the SGD and downstream at the compressor inlet is shown in terms of velocity fields in Fig. 9a–d for four vane positions and a pressure drop of 1500 Pa; the light areas represent maximum velocities of about 33 m/s and the dark areas minimum velocities of stagnating or re-circulating flow. At the top-left and bottom right of each figure, cross-section views of the flow distribution corresponding respectively to the inducer inlet section and to the SGD inlet section can be seen. Fig. 9c and d show that the flow downstream of the SGD has a perfect radial distribution due to the high level of swirl generated in the device. Hence, the effective flow passage area is annular and most of the flow is concentrated in the periphery of the duct. This means that the closing of the SGD vanes has the effect of reducing the effective flow passage section at the compressor inducer inlet, as has also been confirmed with the experimental results from the flow test rig (Fig. 3c). This annular flow distribution is less evident in the SGD cases of 15° and 30° vane aperture. Nevertheless, it is possible to identify this effective area by

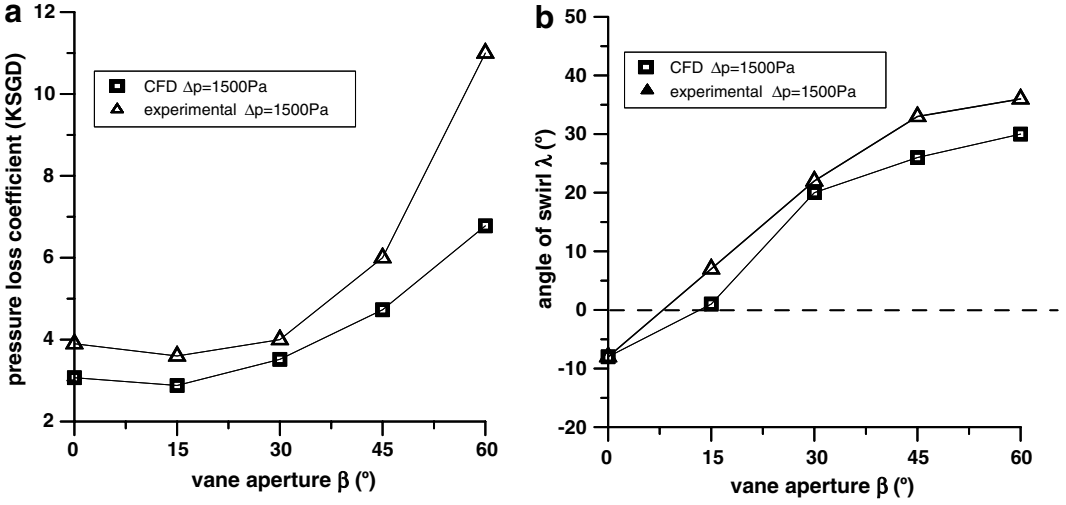

Fig. 8. Comparison of the SGD characterization with the CFD calculations: (a) pressure loss coefficient, (b) swirl.

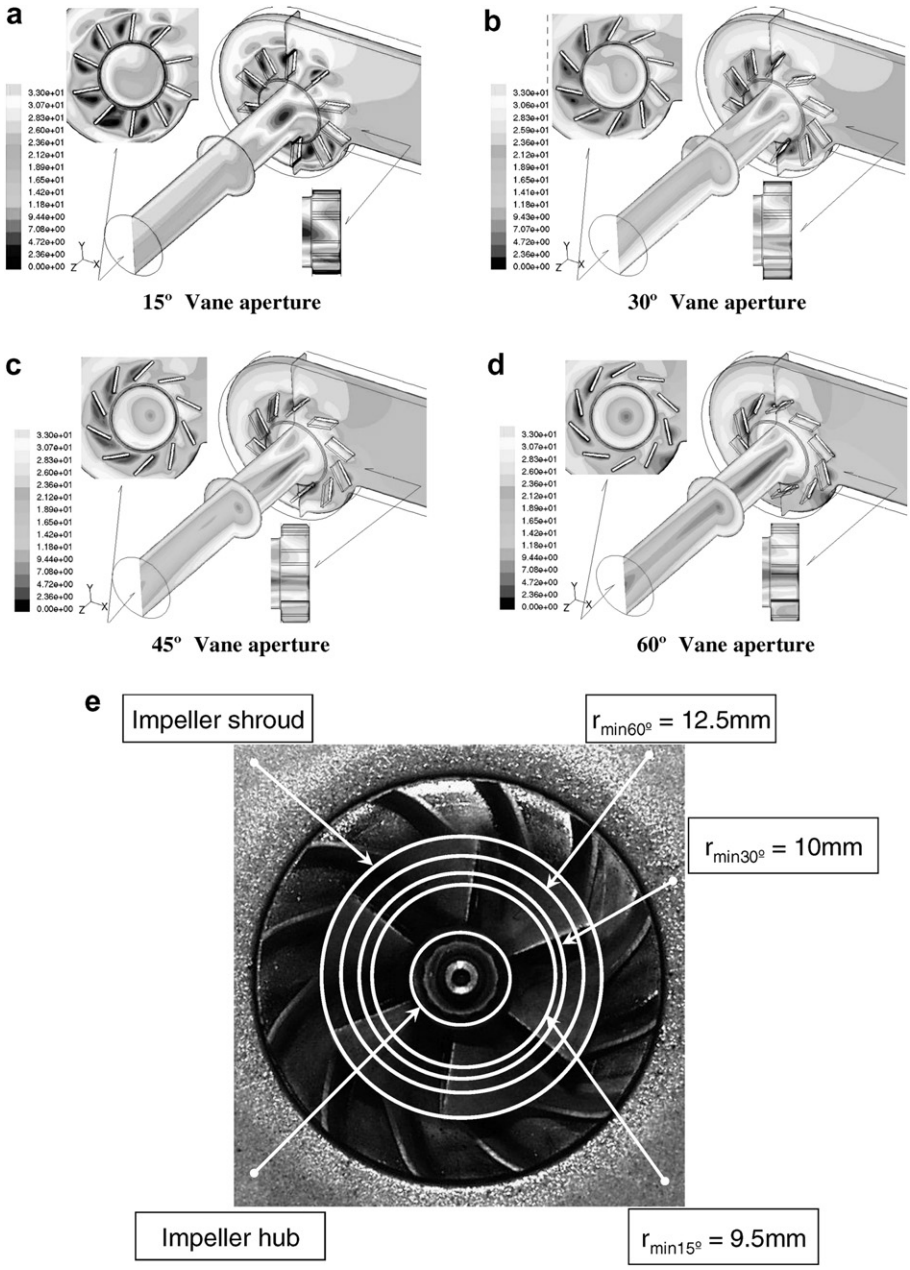

Fig. 9. Velocity field (m/s) for a pressure drop of 1500 Pa at 15° (a), 30° (b), 45° (c) and 60° (d) of β angle. (e) Effective flow passing areas for each value of vane aperture.

defining the flow passage section from the inducer shroud (maximum radius) to a given minimum radius determined by the coefficient of effective flow passing section (c_D), defined in Eqs. (5) and (6). The calculated effective sections are represented in Fig. 9e, which shows the minimum radius for each vane aperture.

6.2. Reconstruction of the velocity triangle at the compressor inducer

In order to better explain the modifications of the line that limits the surge region with negative and positive pre-rotation, the velocity triangles at the inducer inlet have been reconstructed. The air flow pattern predicted by the CFD study at the SGD outlet has been used to obtain the variables necessary for drawing the velocity triangles at the inducer inlet. According to the CFD solutions, the air mass flow distribution is different at the impeller entry section for each position of the SGD vanes and the flow passing in the impeller is concentrated at the periphery of the inlet section (Fig. 9e).

Since the effective section at the impeller is thus known, the average axial component of the speed (C_{1a}) can be determined using continuity. (C_{1a}) is taken as the circumferentially averaged axial component of the velocity in the middle point between the impeller shroud and the r_{min} of each vane aperture (Fig. 9e). The swirl angle can be calculated at the same middle point (λ_{middle}) assuming a linear

variation of the swirl, from λ at the impeller shroud, defined by Eq. (11), to 0 at r_{min}, where it has been assumed that the tangential component of the velocity (C_{1u} in Fig. 6) is zero. The tangential component (C_{1u}) can then be calculated from C_{1a} and λ_{middle} using Eq. (11). The linear velocity of the rotor (U_1) together with C_{1u} and C_{1a} define the vectors of the velocity triangle, as shown in Fig. 6. Hence W_1 can be calculated and the value of the approach angle (ϕ) is obtained from Eq. (16):

$$\phi = \operatorname{arctg}\left(\frac{C_{1a}}{U_1 \pm C_{1u}}\right) \tag{16}$$

The angle of attack (g) defined in Fig. 6 is also variable with the radius of the blade inducer from the hub to the shroud. With the help of a digitalization machine one of the rotor inducer blades was digitally processed to obtain its law of variation. Following the definition by Japikse (1996), the incidence angle (i) is determined by Eq. (17) applied at the middle radius between the impeller shroud and the r_{min} for each SGD vane aperture.

$$\hat{i} = \hat{g} - \hat{\phi} \tag{17}$$

The reconstruction of the incident angle i is supported by the good agreement shown between the experimental measurement in the flow test rig and the CFD studies (Fig. 8b). The reconstruction of the velocity triangles has been performed for ±15°, ±30° and ±60° SGD vane apertures but only for the points that limit surge region. The incidence angle and the relative velocity have been plotted versus the wheel rotating speed in Fig. 10 and compared with the corresponding values in the axial inlet configuration. The negative (Fig. 10a and c) and positive (Fig. 10b and d) SGD configurations have been separated. The results show in general that W_1 is higher with the negative β configuration (Fig. 10a) although lower angles of incidence are generally obtained in the case of positive β angles (Fig. 10d). Therefore, the effect of the relative velocity is more important for shifting the surge-limit line. Indeed, the flow can better overcome the resistive pressure downstream of the compressor when W_1 is large, so that the fluid in the impeller becomes more stable and the stall phenomenon is delayed. The previous conclusion is especially evident in the case of −60° vane aperture. It is also worth noting that, although the surge-limit points have lower air mass flow rates in the −60° case (Fig. 4a), hence lower C_{1a}, W_1 is higher than for the points with positive β angle (Fig. 10a and b).

Considering that the surge limit points represented in Figs. 4 and 5 are very similar because the influence of pressure losses is not very significant at these low air mass flows, and that Fig. 10 only shows these surge limit points, it is also possible to analyse the changes observed in the isentropic efficiency with the ±60° vane configurations for these points (Fig. 4g and h). On the one hand, the improvement in efficiency observed in Fig. 4h for the +60° case is caused by the high reduction in the i angle with respect to the axial configuration (Fig. 10d). On the other hand, Fig. 10c shows that the i angle is also reduced in the case of −60° SGD aperture with respect to the axial configuration. Indeed, though ϕ decreases with the increment of the negative pre-rotation, the flow is concentrated in the periphery of the compressor inducer, where g is minimum, therefore i is also reduced with respect to the axial configuration (Eq. (17)). In spite of this, the efficiency is not improved in the negative case (Fig. 4g). Nevertheless, the efficiency is quite similar to the axial configuration. Therefore, the operation of the compressor becomes stable

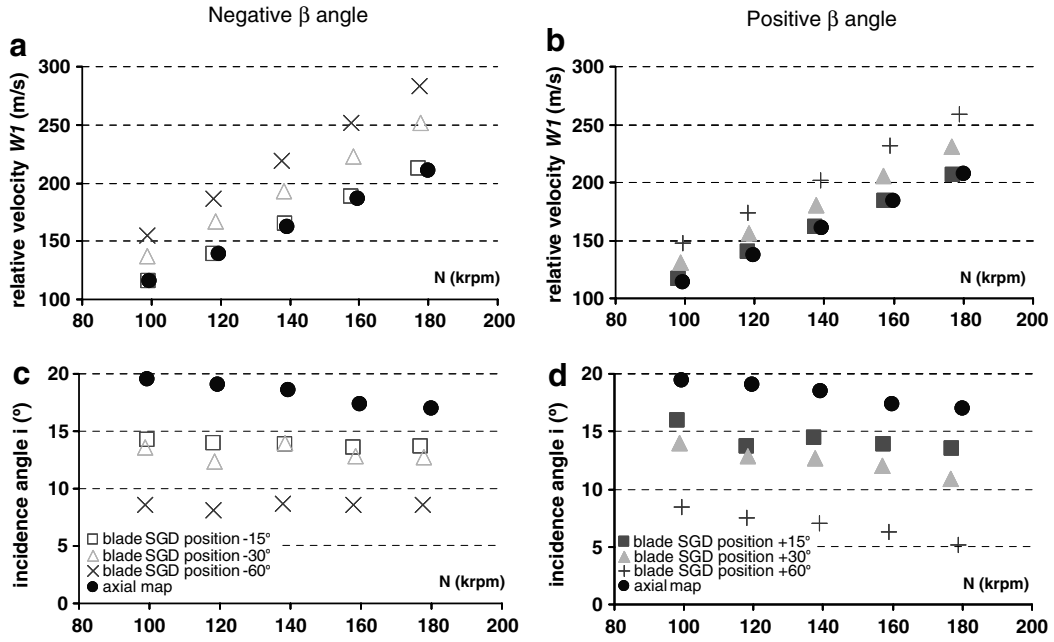

Fig. 10. Incidence angle (i) and relative velocity (W_1) calculated for points of the surge limit line with negative and positive SGD vanes angle (β).

and the surge-limit point is shifted, especially at 180 krpm (Fig. 4a).

It is worth highlighting several aspects concerning the analysis of the results. The first one is that the hypothesis of radial flow distribution in the periphery of the inducer is not really fulfilled for low β angles, i.e. at values of 15°, as can be observed in the flow patterns in Fig. 9a and b. The second one is that the analysis performed is also less true if the air mass flow rate is lower than 0.025 kg/s. As mentioned in the previous sections, for mass flow rates under this value the measurements of the swirl produced by the SGD are uncertain due to the low momentum of the flow. The minimum flow occurs at low speed near the surge limit line. However, in the case of −60° SGD vane aperture, for which the best improvement of the surge line was obtained, there are no uncertainties due to the above-mentioned aspects.

Finally, it is also worth noting that although the CFD calculations do not take into account the effect of the impeller, the phenomenon that it is being calculated is well represented with this simple approach. The points shown in the line that limits the surge region, obtained following the criteria exposed by Galindo et al. (2006), are still fully stable points. Therefore, even if there could locally be some reverse flow it is not dominant and the momentum of the inlet flow is high enough to overcome the upstream influence of the rotating impeller in the flow field. The authors have performed some CFD calculations with a simplified impeller geometry at the SGD outlet. Two configurations have been calculated, 30° and 60° of β value, at the operative conditions given by the stable points that limit the surge area at 180 krpm. The solution at the impeller inlet shows that the swirl (λ) changes by about 30% with respect to the values of Fig. 8b. However, since the mass flow near the surge limit is low, the value of C_{1a} is very small compared to U_1, especially at high rotating speed. Hence, the differences obtained in the calculated incidence angle (i) with respect to simpler calculations without the impeller (Fig. 10c) are lower than 2%.

7. Summary and conclusions

From this study it can be concluded that the SGD improves the surge limits when the flow pre-whirl has the opposite direction to the compressor rotation. It is worth noting that while most of the known pre-whirl devices (Nikpour, 2004; Pampreen, 1993; Whitfield et al., 1991) are based on an axial inlet flow and guide vanes (IGV), the SGD system presented here has a radial inlet and centripetal vanes. This difference strongly conditions the flow field at the compressor inlet. The main difference lies in the special flow distribution, with low velocities at the centre and high velocities at the periphery of the compressor inducer. On the one hand, this reduces the effective passage section and strongly increases the relative velocity of the flow and on the other hand, it concentrates the flow in a zone of the inducer where the angle of the blades (g) is minimum.

Therefore, whilst the IGV principle of operation is based only on using positive swirl to increase the approach angle (ϕ), thus reducing the incidence angle (i) to delay the stall in the compressor blades, the SGD concept is based on two aspects. On the one hand with the negative swirl the relative velocity (W_1) of the flow at the inducer inlet is increased with respect to the positive swirl. This increment is even higher than with IGV devices due to the reduction of the effective section and the consequent increment of the axial velocity (C_{1a}). On the other hand, the flow incidence angle (i) is reduced with respect to the axial configuration even with the negative swirl due to the reduction of g in the periphery of the compressor inducer, where the flow is concentrated by the SGD with the −60° configuration. With the positive swirl the incidence angle (i) is much more reduced than with negative and some improvements in surge margin have also been presented. Nevertheless, the combination of excellent relative velocities (W_1) and incidence angles (i) lower than with axial inlet configuration makes the negative configuration the optimum. In addition, the negative pre-whirl produced with the SGD device allows obtaining higher compression ratios than the positive pre-whirl, so that the negative configuration of the device is recommended in spite of its lower isentropic efficiency.

By replacing a 90° elbow by the SGD, there is no severe deterioration of the compression ratio performance. This is illustrated by the −15° of SGD vanes position case. Indeed, it is probable that the optimum position of the vanes lies somewhere between −15° and 0°. In addition, this study shows that it is possible to shift the surge limit so as to obtain a maximum improvement in boost pressure of about 0.45 bar with an SGD vane aperture of −60° at very low air mass flow rates for a given reciprocating internal combustion engine. Indeed, it is possible to combine both positive characteristics, the low loss in compression ratio and the increment of the surge margin, by closing the SGD vanes from −15° to −60° when the internal combustion engine is working in the zone of the compressor map with low air mass flow rate and high compression ratio, and opening again the SGD from −60° to −15° when the engine is working outside this zone. A mechanism that controls the SGD vanes in function of the reciprocating internal combustion engines operative conditions would therefore be mandatory in order to use the SGD for improving the turbocharger performance.

The SGD configuration, with a 90° compressor inlet, allows solving the packaging problem stated in Section 1 with the only requisite of ensuring that the inlet cross section area is equal to the outlet cross section area. Indeed, the practical feasibility of including the presented design of SGD within the limited space available for the engine and its accessories is guaranteed because the width of the square inlet section can be reduced by increasing its height in order to adapt the SGD to the available room.

Since this study has been performed with a typical turbocharger, used in passenger car engines from 1.9 to 2.2 l of displacement, and the concept of the SGD design is

general enough, the present findings can be extended to applications ranging from centrifugal compressors used for turbocharging heavy-duty Diesel engines, of about 12 l displacement, up to actual downsized high speed Diesel engines, of about 1.4 l displacement. With respect to the engine speed/load range: if the initial matching between the compressor, without the SGD, and the internal combustion engine is acceptable, the SGD would be beneficial in whatever speed or load range of the internal combustion engine. Indeed, solutions have been presented that allow the SGD to work well in all zones of the compressor map.

In summary, the SGD is a good solution to the problem of finding a device that allows packaging the compressor with a 90° inlet. This is not possible with conventional IGV mechanisms, since these affect the global performance of the turbocharger at mean and high air mass flow rates. In addition, by installing a variable actuation mechanism for the SGD vanes the flow pre-rotation can be used to control the centrifugal compressor, thus providing the possibility to increase the surge limit at lower air mass flow rates and higher compression ratio. Finally, it is interesting to highlight the feasibility of the proposed mechanism that should be completely equivalent to those used for moving the stator blades in the variable geometry centripetal turbines (VGT) from the turbochargers. In the VGT, this mechanism allows changing the angle of incidence of the flow leaving the stator through the rotor and is controlled via a pressurized air circuit generally available on the engine auxiliary elements. In the SGD the mechanism would not suffer any thermal stresses and could be made with cheaper and lighter materials.

References

Araneo, L., Coghe, A., Cossali, G.E., Brunello, G., 1999. Experimental investigation of gas density effect on diesel spray penetration and entrainment. SAE paper 1999-01-0525.

Arcoumanis, C., Whitelaw, J.H., 1987. Fluid mechanics of internal combustion engines – a review. Proc. IMechE 201 (C1).

Ariga, I., Kasai, N., Masuda, S., Watanabe, Y., Watanabe, I., 1983. The effect of distortion on the performance characteristics of centrifugal compressor. ASME J. Eng. Power 105, 223–230.

Ariga, I., Masuda, S., Ookita, A., 1987. Inducer stall in a centrifugal compressor with inlet distortion. ASME J. Turbomach. 109, 27–35.

Binder, K., Schwarz, V., 2004. Present and future of heavy duty engines strategies for compliance to the emission legislation. In: Thermo- and Fluid Dynamic Processes in Diesel Engines 2: Selected Papers from the THIESEL 2002 Conference Valencia, Spain. Springer-Verlag, ISBN 3-540-20187-4, pp. 19–28.

Chen, H., Connor, W., 2002. Turbocharger compressor developments for passenger car gasoline engine applications. IMechE 216.

Coppinger, M., Swain, E., 2000. Performance prediction of an industrial centrifugal compressor inlet guide vane system. IMechE 214 (Part A), 153–164.

Desantes, J.M., Benajes, J., Urchueguía, J., 1995. Evaluation of the non-steady flow produced by intake ports of direct injection Diesel engines. Exp. Fluids 19 (1), 51–60.

Elder, R.L., Gill, M.E., 1985. A discussion of the factors affecting surge in centrifugal compressors. ASME J. Eng. Gas Turbine Power 107, 499–506.

Fink, D.A., Cumpsty, N.A., Greitzer, E.M., 1992. Surge dynamics in free-spool centrifugal compressor system. ASME J. Turbomach. 114, 321–332.

Galindo, J., Serrano, J.R., Guardiola, C., Cervelló, C., 2006. Surge limit definition in a specific test bench for the characterization of automotive turbochargers. Exp. Thermal Fluid Sci. 30, 485–496.

Gu, F., Engeda, A., Cove, M., Di Liberti, J.L., 2001. A numerical investigation on volute/diffuser interaction due to the axial distortion at the impeller exit. ASME J. Fluids Eng. 123, 475–483.

Hansen, K.E., Jørgensen, P., Larsen, P.S., 1981. Experimental and theoretical study of surge in small centrifugal compressor. ASME J. Fluids Eng. 103, 391–395.

Hunzinker, R., Dickmann, H.P., Emmrich, 2001. Numerical and experimental investigation of a centrifugal compressor with an inducer casing bleed system. IMechE 215 (Part A), 783–791.

Japikse, D., 1996. Centrifugal Compressor; Design and Performance. ISBN 0-933283-03-2. Concepts ETI, Inc.

Kim, Y., Engeda, A., Aungier, R., Derinzi, G., 2001. The influence of inlet flow distortion on the performance of the centrifugal compressor and development of an improved inlet using numerical simulations. IMechE 215 (Part A), 323–338.

Kyrtatos, N., Watson, N., 1980. Application of aerodynamically induced prewhirl to small turbocharger compressor. ASME J. Eng. Power 102, 934–950.

Ludtke, K., 1983. Aerodynamic tests on centrifugal compressors – the influence of the vaneless diffusor shape. ASME J. Eng. Power 105, 902–909.

Luján, J.M., Bermúdez, V., Serrano, J.R., Cervelló, C., 2002. Test Bench for Turbocharger Groups Characterization. SAE 2002-01-0163.

Meherwan Boyce, P.E., 2002. Centrifugal Compressors: A Basic Guide. Pennwell Corp.

Nikpour, B., 2004. Turbocharger compressor flow range improvement for further heavy duty diesel engines. In: Proceedings of Thiesel-2004 Conference. Thermo- and Fluid Dynamic Processes in Diesel Engines. ISBN 84-9705-621-3, pp. 125–143.

Pampreen, R.C., 1993. Compressor Surge and Stall. Concepts NREC. ISBN 0-933283-05-9.

Pan, D., Whitfield, A., Wilson, M., 1999. Design considerations for the volutes of centrifugal fans and compressors. IMechE 213 (Part C), 401–410.

Qi, D.T., Pomfret, M.J., Lam, K., 1996. A new approach of the design of fan volute profiles. IMechE 210, 287–294.

Schulte, H., Schorn, N., Kindl, H., Serrano, J.R., Margot, X., Donayre, C., 2004. Influence of various compressor inlet designs on compressor performance. In: Proceedings of Thiesel-2004 Conference. Thermo- and Fluid Dynamic Processes in Diesel Engines. ISBN 84-9705-621-3, pp. 103–116.

Supercharger Testing Standard, 1995. SAE J1723 ISSUED AUG95. Society of Automotive Engineers, Inc.

Talib, Z., Farge, Johnson, Mark W., 1992. Effect of flow rate on loss mechanisms in a backswept centrifugal impeller. Int. J. Heat Fluid Flow 13 (2), 189–196.

Tange, H., Ikeya, N., Takanashi, M., Hokari, T., 2003. Variable geometry diffuser of turbocharger compressor for passenger vehicles. SAE Paper 030151.

Theotokatos, G., Kyrtatos, N.P., 1997. Diesel engine transient operation with turbocharger compressor surging. SAE Paper 970344.

Turbocharger Gas Stand Test Code, 1995. SAE J1826 REAF. MAR95. Society of Automotive Engineers, Inc.

Watson, N., Janota, M.S., 1982. Turbocharging the Internal Combustion Engine. MacMillan Publishers Ltd, ISBN 0 333 24290 4.

Whitfield, A., Wallace, F.R., Atkey, C., 1975. Experimental and theoretical performance of a radial flow turbocharger compressor with inlet pre-whirl. IMechE 189, 43/75.

Whitfield, A., Sutton, A.J., Leonard, H.J., 1991. The development of turbocharger compressors with improved surge margin. IMechE C433/063, 9–18.